

UHV transmission electron microscopy of Ir(001)

II. Atomic positions of the (5×1) reconstructed surface from HREM and R -factor refinements

L.D. Marks, P. Xu and D.N. Dunn

Department of Materials Science and Engineering, Northwestern University, Evanston, IL 60208, USA

Received 19 January 1993; accepted for publication 25 May 1993

A partial solution of the atomic scale structure of the Ir(001)- (5×1) reconstructed surface is reported combining direct high resolution electron microscopy and R -factor analyses of transmission electron diffraction data. From the high resolution imaging, the structure can be uniquely identified as a hexagonal monolayer on the surface with at most small distortions. R -factor minimization of the near surface structure based upon 8-bit digitization of the diffraction data shows systematic differences for models using single and multiple layers, demonstrating the existence of sub-surface strain fields. Unfortunately, the intrinsic error of 8-bit digital data is too large for a full multilayer minimization. Fitting was also performed using sub-surface relaxations constrained to match analytical strain solutions. These models indicate a two-fold bridge registry of the surface hexagonal layer with a three-fold hollow registry of the sub-surface atoms with respect to the surface layer and small sub-surface relaxations. The data reduction is quantitative with a 20–30% coverage, in agreement with experimental imaging data, and the accuracy of the atomic positions is about ± 0.005 nm.

1. Introduction

The iridium (001) surface is a relatively unique system when considered in terms of epitaxial growth. Many of the fcc (001) metal surfaces (e.g. Au, Pt, Ir) show a reconstruction with a top hexagonal layer (i.e. equivalent to a (111) fcc surface) registered in some complicated supercell [1–3]. Among these systems, only iridium shows a simple (5×1) registry. It is therefore a good test surface for understanding hexagonal-cube epitaxy with a classic Frank–van der Merwe monolayer. Although a number of studies of this surface have appeared [3–7], it is still very unclear what the registry is, or the locations of the atoms. There are two main possibilities which have been described in the literature, namely a two-fold bridge model and a four-fold hollow model [3], as illustrated in fig. 1. The absolute shift between these two is exceedingly small, only about 0.016 nm with an unperturbed hexagonal layer. LEED intensity analyses [4] had found that the bridge model was the preferred one based on the R -fac-

tors, although the Zanazzi–Jona R -factor of 0.34 is too poor to qualify this structure as final, and no attempt was made to go beyond a simple hexagonal surface layer with layer relaxations normal to the surface.

The intention of this note is to present a partial solution of the structure combining direct imaging using high resolution electron microscopy and R -factor analyses of dynamical electron diffraction data. Although most surface structure models consider only the top surface layer, e.g. ref. [4] for Ir(001)- (5×1) , experimental evidence for sub-surface multilayer relaxation was found in various LEED studies on clean metal surfaces [8] and for Pt(001)- (5×20) reconstruction [9]. In our analyses, the sub-surface distortion due to a long range strain field is considered, and we demonstrate that an improved R -factor can be obtained by allowing the bulk layers to relax. Unfortunately the R -factor analysis used 8-bit digital diffraction data, and contained relatively large intrinsic errors even though the number of beams used was very large (up to about

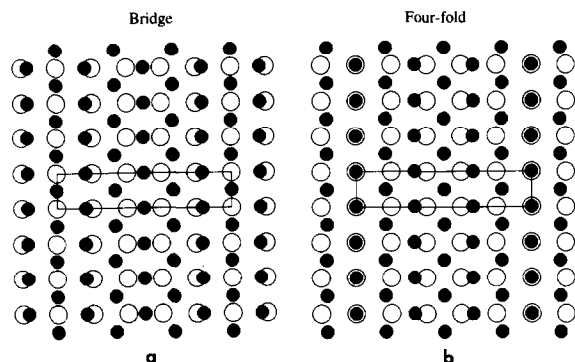


Fig. 1. Schematics of the surface registry of the Ir(001)-(5×1) reconstruction. (a) Two-fold bridge model and (b) four-fold hollow model. Filled circles are surface layer atoms, and open circles are the first bulk layer.

10^3). To prevent unphysical solutions, the fitting was constrained to be of a form which satisfies the solutions of an elastic strain field. With this model, we find that the best model is a two-fold bridge type structure with small surface and sub-surface distortions.

2. Experimental methods

The sample preparation for the reconstructed Ir(001) surface has been described in the previous paper [10]. For the high resolution electron microscopy (HREM), two modes were used. The first was conventional HREM along the (001) zone axis. In this case the scattering is complicated by interference between the surface and bulk lattices. The second was with the crystal tilted off to damp the strong Bragg beams. Within a kinematical approximation (not fully adequate but sufficient for a qualitative explanation), when the crystal is tilted off, the reciprocal lattice spikes (or rel-rods) from the surface structure drop relatively little compared to the reduction in the bulk scattering, and the images can be directly interpreted in terms of the surface atomic structure. Except for extreme care to correct beam tilt and astigmatism, no special techniques were used for these images; HREM images were taken with 3–4 seconds exposure at magnifications of 500 000–700 000.

For the electron diffraction data, a series of patterns were recorded at different exposures. The absolute levels of some of the stronger diffracted beams were determined using electron energy loss spectroscopy [11]. The diffraction patterns were digitized to 8-bits using an Optronics C1000 microdensitometer and then analyzed using SEMPER software on Apollo workstations – more details are provided below. It should be mentioned that the photographic film was calibrated to be linear over the range used herein.

3. Results

3.1. HREM

We will first describe the HREM results, since these severely constrain the possible surface structures. Figs. 2 and 3 show, respectively, HREM images taken on the zone axis and off the zone axis. On the zone axis the images are very complicated, the strongest contribution coming from the bulk {200} diffraction and moiré fringes due to the reconstructed surface, and some contribution from the {110} or surface $\{1 \times 1\}$ diffraction spots. (It is not obvious from the images that all of these are present, but they show up clearly in power spectra.) Analysis of the on-zone images using multislice calculations unfortunately failed to provide much useful information, mainly because the off-axis data was far more directly interpretable. It was possible to match the experimental images fairly well, but not to constrain the registry of the reconstruction substantially. As mentioned earlier, the difference between the two primary registries is only 0.016 nm, too small to be determined with sufficient confidence. It should be noted that it was rare to see two overlapping orthogonal domains in dark field images (part I), indicating that the reconstruction was generally a partial coverage of both surfaces.

The off-axis images were far simpler to interpret since bulk contrast was greatly reduced. The images consisted either of a simple, almost perfect, hexagonal lattice, or a slightly more complicated structure with the full long repeat distance in the “5” direction. The former could be inter-

preted as regions where the total bulk thickness is an integer number of unit cells, so the $\{1 \times 1\}$ lattice is essentially invisible [12]. When there is an incomplete number of cells in the specimen thickness, moiré fringes between the $\{1 \times 1\}$ diffraction spots and the surface hexagonal layer diffraction are visible. These two regions can be seen in fig. 3 separated by a step.

It is important here to point out that the HREM data severely restricts the range of possible surface structures. For instance, the surface cannot be substantially different from a simple hexagonal layer, since if it was, there would be far more detail in the images. Therefore, many exotic structures can be immediately excluded from consideration. In the on-zone high resolution images (e.g., fig. 2), the full "5" period is clearly visible, which correlates with the diffraction data shown below.

3.2. Diffraction

Diffraction data at two different orientations were analyzed in some detail: one close to a zone axis shown in fig. 4a and another tilted off the zone shown in fig. 4b. For both cases the exact orientation was determined from Kikuchi lines: the on-zone pattern has a small 9.6 mrad tilt, the tilt for the off-zone pattern is 112 mrad. The thickness was estimated from both the intensity of the plasmon scattering in electron energy loss spectroscopy and by matching the bulk intensities using full multislice calculations of the dynamical diffraction. Both methods indicated a specimen thickness of about 18.6 ± 2 nm.

An example of the raw data reduced to a line scan across some of the diffraction spots is shown in fig. 5. Intensity values were obtained by removing the background using a high-pass filter, and

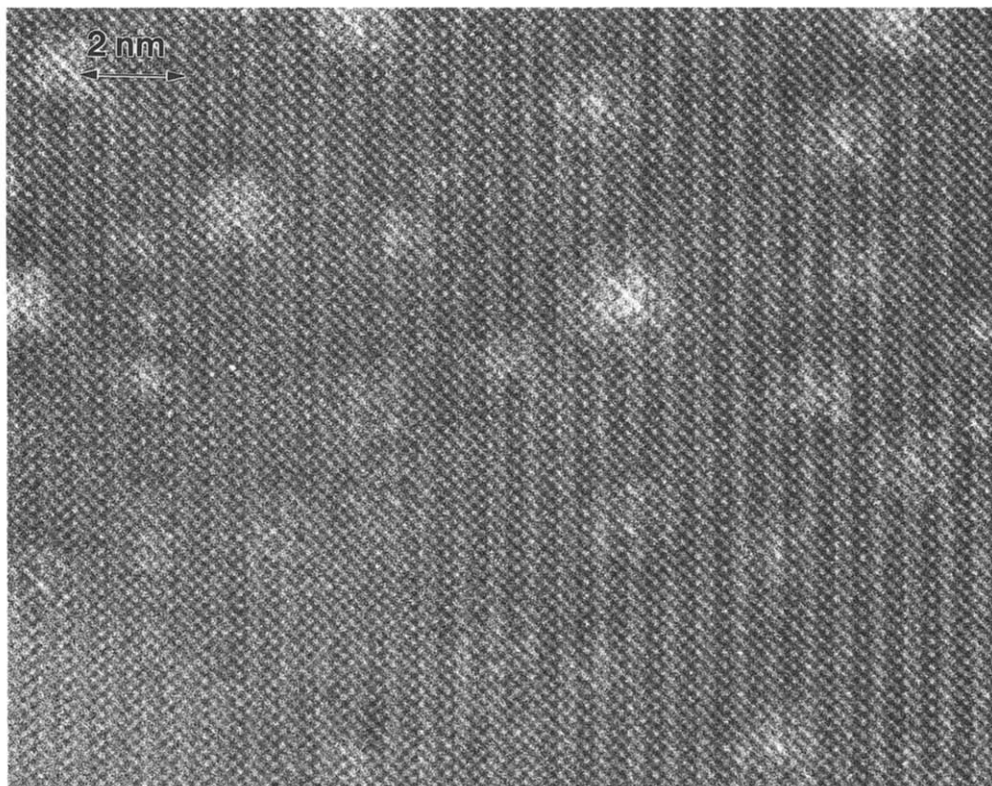


Fig. 2. High resolution image of the Ir(001)-(5 × 1) reconstruction taken with the sample on the (001) zone axis.

then by integrating the intensity around each surface cell spot. Two sets of data (from the two orthogonal reconstruction domains) were obtained for each pattern. Typically, one set of data contains more than 200 beams. A partial list of the intensities for the on-zone and off-zone cases is shown in table 1.

Several fine points are buried in a numerical analysis, and three will be pointed out here. A systematic point to note is that intensity values are larger when $h + k = 2n$ (h and k are surface

diffraction indices in the (5×1) unit cell notation), and smaller, but non-zero when $h + k = 2n + 1$. This is consistent with the imaging results, i.e. the full "5" period is visible along with the strong half "5" period. Whereas one might explain all the $h + k = 2n$ spots as a consequence of double diffraction between a hexagonal monolayer and the bulk crystal, the odd-order spots cannot be explained this way. Second, although the simple hexagonal monolayer spots are the strongest ones, the remainder of the spots *cannot*

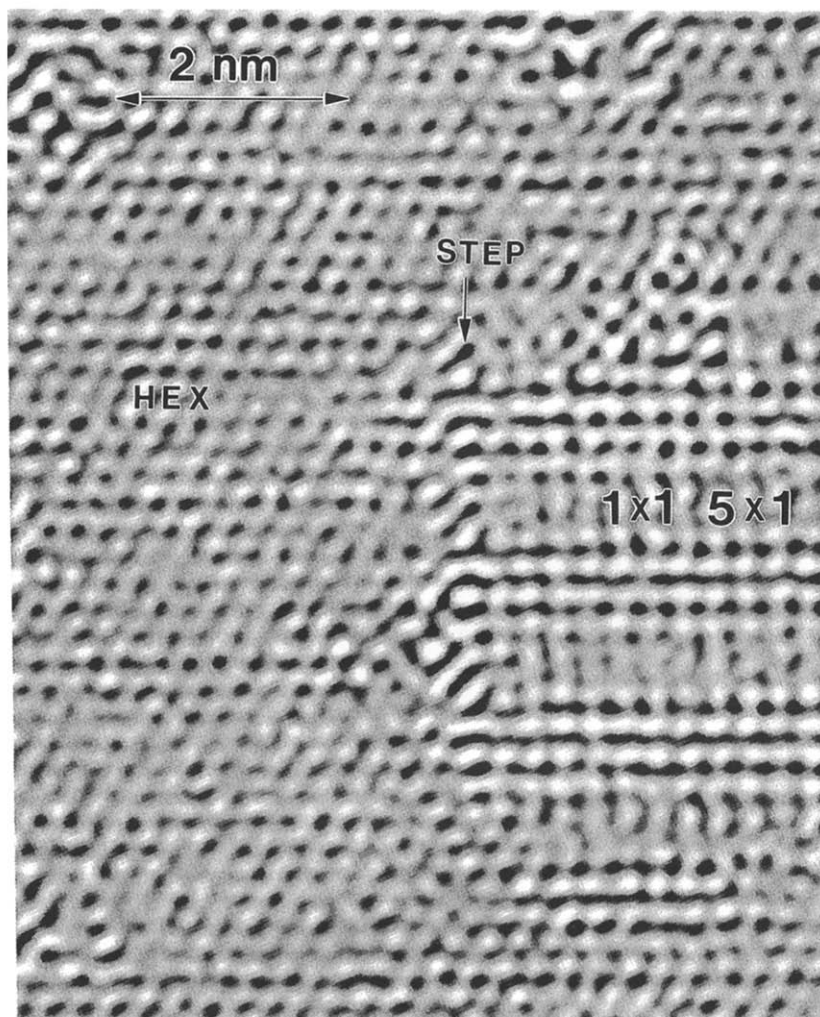


Fig. 3. High resolution image of the Ir(001)-(5 × 1) reconstruction taken with the sample tilted off the (001) zone axis. The left side of the step shows the surface hexagonal layer structure and the right side shows the moiré fringes between the hexagonal lattice and the {1 × 1} lattice.

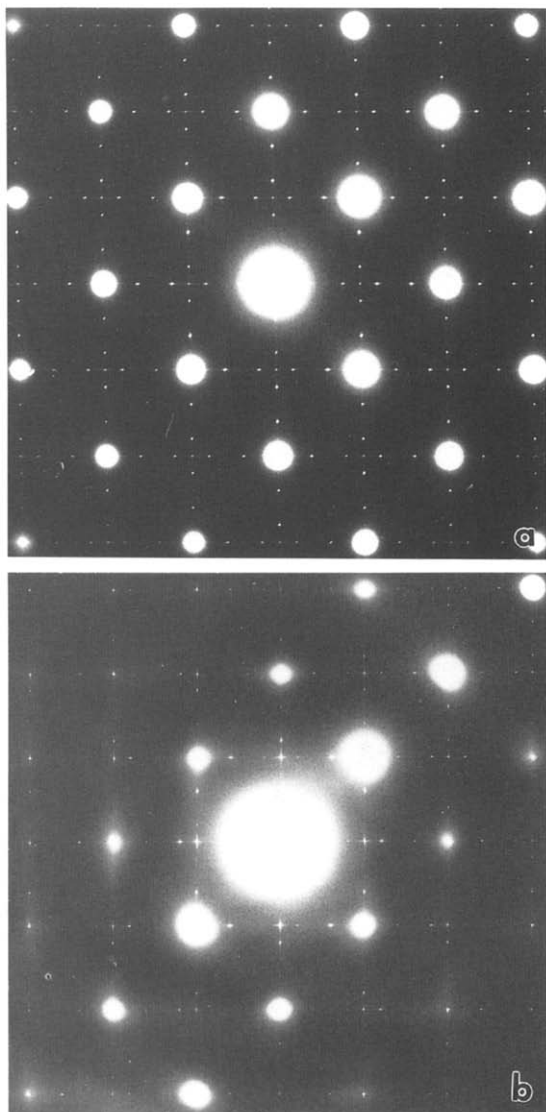


Fig. 4. Selected area diffraction patterns of the Ir(001)-(5×1) reconstruction. (a) Near the zone axis and (b) off the zone axis. The patterns were digitized into an 8-bits form using a microdensitometer for further analysis.

be explained simply by double diffraction – they are too strong. Some distortion of the structure beyond a simple hexagonal layer on a perfect substrate is necessary to explain the data. Finally, we should note that the experimental intensities do not have, for instance, an inversion center. In the off-zone data, the difference in intensity be-

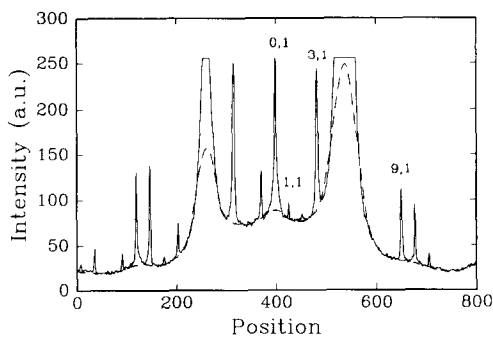


Fig. 5. Line scan (solid line) from a row of diffraction spots in the digitized pattern of fig. 4b. The background was fitted (broken line) with a high pass filter and subtracted from the raw data before integration.

tween (hk) spots is about a factor of 2–5. This is to be expected since the symmetry of any diffraction pattern is only the combined symmetry of the

Table 1

A partial list of the intensity values for the on-zone and off-zone diffraction patterns; the absolute intensity values were determined by the EELS measurements of some of the stronger diffraction spots, e.g., $I_{\text{abs}}(3, 1) = 4.76 \times 10^{-4}$ for on-zone, $I_{\text{abs}}(3, 1) = 1.35 \times 10^{-5}$ for off-zone

h, k	Intensity (on zone)	Intensity (off zone)
4,0	36.6	1.93
6,0 *	77.6	69.7
7,0	3.46	3.15
8,0	82.6	7.00
12,0 *	58.2	25.1
13,0	0.59	1.55
1,1	34.6	3.23
2,1	0.70	Very weak
3,1 *	89.7	72.5
7,1	55.0	Very weak
8,1	1.21	Very weak
9,1 *	44.7	34.0
2,2	34.9	4.49
3,2	2.02	1.62
4,2	35.2	2.10
6,2 *	52.2	20.1
7,2	2.31	2.23
8,2	28.3	4.16
1,3	15.0	2.10
2,3	1.07	Very weak
3,3 *	27.5	9.25

* Hexagonal spots; the spots which were too weak to measure were assumed to be zero in the fitting.

crystal and incident beam; this is handled by including the correct incident beam direction in the multislice calculations.

3.3. *R-factor minimization*

Some preliminary analyses of the data were performed using a simple kinematical form to fit the off-zone pattern as has been suggested by previous workers, e.g., refs. [13,14]. However, the *R*-factors were quite poor and the atomic positions unreasonable; these analyses yielded a near-perfect hexagonal layer fitting the strong hexagonal spots fairly well but not fitting anything else. From our previous theoretical analyses [12,15] we know that kinematical models are inadequate, and in any case they are unnecessary since with care sufficient information can be obtained for accurate dynamical analyses. (In work in progress on the Si(001)-(2 × 1) surface we have found that totally spurious results can be produced with kinematical approximations. It should be noted that in fig. 4b of the companion paper there are variations of the surface spot intensities across the diffraction discs, as expected for dynamical diffraction.)

Using the thickness and tilt data mentioned above, the experimental intensities were matched to calculated intensities using full dynamical multislice simulations [16–18] for the reconstruction on the top and bottom surfaces; a linear combination of the two intensities was used. For reference, the *R*-factor used for all the calculations was a standard unweighted form:

$$R = \left[\sum (I_e - c_t I_t - c_b I_b)^2 / \sum I_e^2 \right]^{1/2}, \quad (1)$$

where I_e are the experimental intensities, I_t and I_b are the calculated intensities with the reconstruction on the top and bottom surfaces, respectively, and c_t and c_b scaling constants. (When the fitting was performed to multiple data sets the squares of the *R*-factors were added. It should also be noted that with random superposition of domains, an incoherent addition is correct rather than a coherent addition. Since the absolute intensities of the surface spots are small, double diffraction of the top surface by the bottom sur-

face is a very small effect which can be safely neglected within the accuracy of the experimental data.) A variety of different models and approaches were used as will be detailed below. The original minimizations were performed using the routine LMDIF from Netlib [19]; later calculations used a version of NL2SOL from the port library of the same source [20]. We will first describe the results from minimizations using free variations of the atomic positions, and then rather more rigorous minimizations.

It is appropriate to comment, briefly, upon the reliability of the multislice approach. All the calculations were performed with sampling out to about 60 nm⁻¹, with thin slices of half the [100] repeat distance. It is well established that the technique is exact to the limits of correct modelling of the inelastic potential, and can with care be used to obtain good matching to thermal diffuse scattering [21]. (Several authors, e.g., refs. [22,23], have confirmed consistency between multislice and Bloch wave (e.g., ref. [24]) forms in both transmission [22,23] and reflection [23] with sufficiently large reciprocal space sampling, small slice thicknesses and imaginary potentials. Of the two, multislice is somewhat faster for the type of problems being considered here. The quantitative agreement of Bloch wave theories with experimental data is very well established, e.g., ref. [25]. A recent review of some aspects of these calculations can be found in ref. [26].) We have previously confirmed that there are no complications with using it in a straightforward fashion for surfaces [12,15]. As part of this work various constant multiplicative imaginary terms for the optical potential between 0.1 and 0.01 were tested, as well as a more rigorous recent analysis of the phonon inelastic contribution [27]; the results in terms of the atomic positions were insensitive to these for the off-zone case (see the discussion later for the on-zone case) although there were slight changes in the *R*-factors.

Model set 1

The first set of minimizations were performed using free variability of the atomic positions in the surface and for a number of different layers below this. Most of these calculations were per-

Table 2
R-factors with unrestricted multilayer relaxations

Layers	Parameters	Data sets	Zone	R-factor
1	12	1	Off	0.29
2	22	1	Off	0.21
3	32	1	Off	0.19
4	42	1	Off	0.16
1	12	1	On	0.46
2	22	1	On	0.42
3	32	1	On	0.38
2	22	2	Off	0.21
2	22	2	On	0.49
2	22	4	Both	0.37

formed using just one domain from the diffraction patterns, a few from both domains and one combining both on- and off-zone data. When both domains were used, multislice calculations had to be performed for each, since the orientation of the domain with respect to the specimen tilt was different. Results are summarized in terms of the number of layers used, the R -factor calculated and the number of data sets in table 2.

The deviation between the experimental and calculated data improved as the number of layers increased, e.g., the R -factor with the off-zone data reduced from 0.29 to 0.16 when the number of layers increased from one to four. Based solely on the number of diffracted beams used these improvements appear to be statistically significant [28], and therefore it implies the presence of multilayer relaxations. However, even with many layers, the agreement is poor considering that the accuracy of the theoretical calculations is in principle very high. For all cases, the constants c_t and c_b obtained correlated with a surface coverage of about 20–30%, consistent with the experimental data, so the error level cannot be ignored.

The problem is that with an 8-bit digitization, a typical intensity has a value of about 100 with a (pessimistic) error of ± 1 . With these errors, the unweighted R -factor in eq. (1) is an appropriate form, but the base error can be very large; we estimate it to be > 0.18 for the off-zone case and > 0.4 for the on-zone case. This means that there is a significant danger that the multilayer models are unreasonably fitting the measurement errors, rather than the true intensities. In this case one

can legitimately question simple statistical interpretations of a reduction in the R -factor.

To be more rigorous about the analysis, it is necessary to ask whether there is a systematic feature in the experimental data which is consistent with a multilayer relaxation, i.e. sub-surface strains. This in fact is the case. Considering a displacement field $D(\mathbf{r})$, the potential to be used in the dynamical scattering calculations can be written as:

$$V(\mathbf{r}) = \sum V_g \exp(2\pi i \mathbf{g} \cdot [\mathbf{r} + D(\mathbf{r})]), \quad (2)$$

where V_g are the Fourier coefficients for the reciprocal lattice vector \mathbf{g} of the undistorted potential. Provided that the displacements are small, this can be expanded as:

$$V(\mathbf{r}) = \sum V_g [2\pi i \mathbf{g} \cdot D(\mathbf{r})] \exp(2\pi i \mathbf{g} \cdot \mathbf{r}). \quad (3)$$

Since the reconstruction is periodic, the displacement field can be expanded as:

$$D(\mathbf{r}) = \sum \alpha \exp(2\pi i \mathbf{q} \cdot \mathbf{r}), \quad (4)$$

i.e.,

$$V(\mathbf{r}) = \sum V_g (2\pi i \mathbf{g} \cdot \alpha) \exp[2\pi i (\mathbf{g} + \mathbf{q}) \cdot \mathbf{r}]. \quad (5)$$

With a sub-surface strain (displacement) field, there should be a systematic difference between the experimental and calculated data with more intensity at larger reciprocal lattice vectors in the

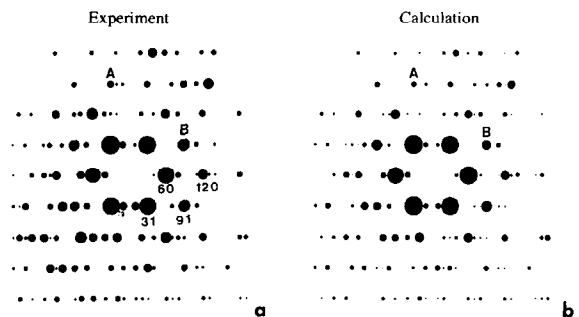


Fig. 6. Schematic showing the systematic discrepancies between (a) the on-zone experimental diffraction intensities and (b) the calculated intensities with only the surface layer relaxation. The size of the circles represents the intensity values: bulk spots are not shown here. Experimental values are larger than the calculated ones at high angles, see spots labelled A and B for comparison. A few of the strong hexagonal spots are also labelled.

experimental cases. This was found to be the case as shown in fig. 6. This could not be explained by a Debye–Waller term; in fact when this was allowed to vary freely for a single layer, the program wanted to make the Debye–Waller term negative.

A sufficient condition exists for sub-surface distortions, but we still have to demonstrate that the results are not overfitting of the data. Unfortunately, inspection of the atomic positions indicated that the structures were of low symmetry and quite unphysical in most cases. They tended to favor the bridge registry, but this was not definitive. They all contained small distortions away from the hexagonal structure, with the displacements of less than 0.02 nm. A test was performed to artificially amplify the primary diffraction spots such as (6, 0) and (3, 1) of the surface monolayer by three times. This forced the monolayer to a near-perfect hexagonal structure, so the lower amplitude of these spots measured experimentally is a proof of some distortion. Cross-referencing back to the HREM data, we know that these distortions cannot be too large.

Model set 2

Due to the large measurement errors, free minimization is leading to unphysical results as the programs attempt to fit these errors. To overcome this problem, the atomic positions need to be constrained to be reasonable. The approach used was to expand the displacements in forms which will automatically satisfy the elastic boundary conditions of a periodic epitaxial layer. Using u and v for the displacements along the long x and short y directions of the reconstruction, and ignoring the z displacements normal to the surface, which the transmission technique is very weakly sensitive to, the general form of the displacement is [29]:

$$u = (A + Bz) \sum_n \exp(-2\pi|q|z - 2\pi iqx), \quad (6)$$

$$v = C \sum_n \exp(-2\pi|q|z - 2\pi iqx), \quad (7)$$

and

$$q = n/L,$$

where L is the period along the “5” direction and n integers.

The displacement in eq. (6) corresponds to a tensile surface wave, that in eq. (7) to a shear surface wave. Both forms decay exponentially into the bulk, and by using a linear combination of coefficients q all possible surface relaxations can be represented. It would arguably be better to expand the displacements as evanescent phonons, but this would require knowledge of the surface dispersion which would be adding another degree of complexity. Considering the symmetry of either the bridge or four-fold structures, rather than the general exponential form, these can be reduced to sine waves. We note that the shear wave in eq. (7) is problematic to justify physically, but cannot ad hoc be ruled out. It should also be mentioned that the “ Bz ” displacement term will not be well represented in the off-zone case, but in principle can be fitted better in the on-zone case. (It represents a longer range strain field which will be more important under strong diffraction conditions.) However, due to the errors in the on-zone data this term was ignored and only the off-zone data was used. (Tests showed that this term was not important for the off-zone case.)

Initial minimizations were performed for the surface monolayer using either both the u and v displacements (total of four variables) or just the u displacements (two variables) and eight values of q out to $10/L$. It was later determined that only values out to $q = 6/L$ were needed. A total of six layers plus the surface layer were allowed to relax. The results are summarized in table 3. We should note that a larger and more accurate data set was used for these minimizations, so the absolute R -factors in tables 2 and 3 should not be

Table 3
 R -factors with a constrained periodic strain form; all the data is for two orthogonal sets of intensities taken from the same diffraction pattern off the zone axis

Layers	Parameters	Shear	Registry	R -Factor
1	2	No	Bridge	0.34
7	8	No	Bridge	0.27
7	16	Yes	Bridge	0.25
1	2	No	Four-fold	0.37
7	8	No	Four-fold	0.33
7	16	Yes	Four-fold	0.33

The total number of beams is 456. Whether the shear modulation described in eq. (7) was used is detailed in the table.

compared. Several points should be made about this data. First, compared to a simple monolayer, there is a statistically significant reduction in the R -factor when seven layers were used. Second, the results for the bridge model are significantly better. Finally, the reduction when adding in the shear displacement is small, and it is difficult to justify this physically.

The final test of the analysis is that the atomic positions should be reasonable. The full data is summarized in table 4, pictorially in fig. 7. The atoms marked A and A' in the surface and the layer underneath, which in the unrelaxed case are very close together, move apart as would be expected. Secondly, the atoms B and B' move such that the second-layer atom is sitting in a three-fold hollow site with respect to the hexagonal surface. Considering that a three-fold hollow is a much more natural bonding site than two-fold bridging

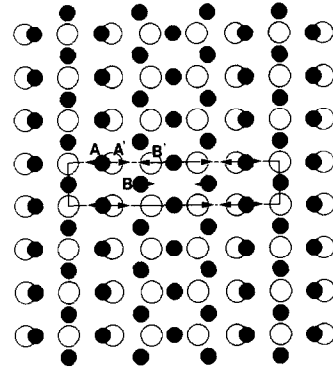


Fig. 7. Structure model of the Ir(001)-(5 \times 1) reconstruction. Periodic strain with only the u displacements was used. Filled circles are surface layer atoms, and open circles are the first bulk layer. (Atomic displacements in the second and subsequent layers are very small.) Atoms A (surface) and A' (bulk) moved apart, and atoms B (surface) and B' (bulk) moved such that B' is in a three-fold hollow site with respect to the surface layer atoms.

Table 4

Atomic positions (in the (5 \times 1) unit cell dimension) derived from the fitting using constrained period strain model; the first two columns are without the shear, the next two with the shear; in all cases the x axis is along the "5" dimension

Layer	x	y	x	y
Hexagonal surface layer	0.000000	0.500000	0.000000	0.500000
	0.159401	0.000000	0.158759	-0.027844
	0.339049	0.500000	0.339277	0.537971
Layer 2	0.000000	0.000000	0.000000	0.000000
	0.205250	0.000000	0.207037	-0.029205
	0.391894	0.000000	0.394733	0.008087
Layer 3	0.102723	0.500000	0.101281	0.509641
	0.293495	0.500000	0.291363	0.476795
	0.500000	0.500000	0.500000	0.500000
Layer 4	0.000000	0.000000	0.000000	0.000000
	0.204172	0.000000	0.199883	0.003963
	0.397823	0.000000	0.397562	-0.014324
Layer 5	0.100876	0.500000	0.099907	0.500499
	0.300501	0.500000	0.299350	0.497671
	0.500000	0.500000	0.500000	0.500000
Layer 6	0.000000	0.000000	0.000000	0.000000
	0.200363	0.000000	0.199817	-0.000427
	0.400112	0.000000	0.399828	-0.000654
Layer 7	0.100092	0.500000	0.099954	0.499892
	0.300120	0.500000	0.299910	0.499725
	0.500000	0.500000	0.500000	0.500000

For reference, the dimensions of the surface unit cell are $A = 1.36$ nm and $B = 0.27$ nm. Only a partial listing is given since the structure has a center of symmetry.

for a hexagonal layer, this is both reasonable and may be a very significant component of the energy minimization of the structure. For both sets of displacements, the movements of the atoms off their "perfect" positions is about 0.01 nm.

A final comment concerns the errors of the analysis. These were very difficult to determine accurately, both numerically and on physical grounds. Numerically we have not been able to adequately obtain the second derivative matrix due to Fourier truncation errors leading to very small, spurious oscillations even with double precision calculations. A more detailed discussion of the errors will be presented elsewhere [30], and based upon a full search of variable space and Monte Carlo simulations the errors in the atomic positions are at most 0.005 nm.

4. Discussion

It is appropriate to discuss, separately, the structural results and the technical aspects of the calculations.

Structurally, we have demonstrated that sub-surface distortions are necessary to explain the experimental data. This is important in that a lot of attention has been placed on the monolayer or interface structure of epitaxial systems and less on the longer range strain fields particularly for surface reconstructions. With a surface reconstruction (or a monolayer thick thin film) a substantial amount of the energy may be locked in the long range strain field. These long range strain fields are small, but appear to be significant. For instance, they adjust the locations of the atoms in the first two layers to give a favorable three-fold bonding of the second layer to the top layer. We would expect long range strain fields to be the rule, rather than the exception, particularly for large cell reconstructions.

Structure analyses by early LEED dynamical calculations [3,4,31] showed that although the buckled bridge model consistently gave a best fit, it was by no means the final structure since the fitting for many beams was very poor [32]. Due to the complexity of the problem, multilayer relaxation was not included. For the purpose of com-

parison, the best fit *R*-factor from these analyses was about 0.4.

In terms of the technical aspects of the calculations and matching to the experimental data, there are some important lessons for the future. One of the most important is that this type of analysis is possible. To our knowledge full dynamical diffraction calculations of such complexity with variable atomic positions have not been attempted before. Calculations were lengthy, typically requiring several days on a 68040 CPU computer, but this is not unreasonable.

The numerical approach can also be improved, and this merits some exploration. For the multi-slice calculations some optimization was performed by saving phase gratings, but further improvements are possible. In particular, we used a finite difference method of calculating the derivatives, but it is possible to calculate these (and second derivatives) directly; this may be a major improvement. We should mention that although intensities based upon single precision representation of the atomic positions were adequate, giving the same results as double precision calculations to a far better accuracy than the experimental data, it is advisable to use double precision for the derivatives.

What appears to be critical is the level of precision of the experimental data. Intensity measurements need to have accuracies of better than 10^{-3} , i.e., 16-bit digitization or $> 10^6$ counts per diffraction spot. Technically these are currently possible, using either slow scan CCD cameras or energy loss spectrometers, and need to be employed more systematically. Energy filtering of the diffraction patterns will also be important since we have found [11] that the major source of background scattering is diffuse inelastic processes. (Such levels of accuracy in the data measurement are standard in other methods of structure determination such as X-ray or neutron diffraction and LEED.)

With better experimental data, it should be possible to exploit as well the on-zone diffraction patterns. Tests indicated that these are very sensitive to the exact specimen thickness and, slightly less, to the inelastic potential employed. Theoretically, on-zone data should be much more sensi-

tive to long range sub-surface relaxations. The off-zone matchings are only weakly dependent upon these, therefore are more robust.

It is also appropriate to discuss a little more the need for dynamical models of the diffraction process, not simpler kinematical models. One of the lessons that we learnt from model set I was that simple minimization of an *R*-factor can lead to unphysical results. During numerous tests with iridium and silicon (001) we have observed that it is often possible to obtain smaller *R*-factors with kinematical models than with a dynamical calculation. This cannot be taken as support for kinematical theory; if the model is inaccurate the results are questionable (GIGO). Kinematical analyses can only be trusted to give approximate atomic positions to, maybe, accuracies of 0.02 nm because of the unknown systematic errors.

With better data collection, and a more complete set of diffraction patterns, we see no reason why atomic positions for multilayers with accuracies of better than 0.001 nm cannot be routinely obtained in the near future. Even with the relatively limited experimental accuracy here, we have quite high precision due to the very large number of experimental intensities that are available to us. One particularly encouraging result is that the quantitative coverage level of 20–30% found from the calculations is in good agreement with the experimental data.

Acknowledgements

We would like to acknowledge support from the Airforce Office of Scientific Research (L.D.M. and P.X.) on grant No. AFOSR-90-0045 and from the National Science Foundation (D.N.D.) on grant No. DMR-85-20280. We would also like to thank Dr. David Bird for providing source code for the imaginary, phonon component of the potential.

References

- [1] S.G.J. Mochrie, D.M. Zehner, B.M. Ocko and D. Gibbs, *Phys. Rev. Lett.* 64 (1990) 2925.
- [2] D. Gibbs, G. Grubel, D.M. Zehner, D.L. Abernathy and S.G.J. Mochrie, *Phys. Rev. Lett.* 67 (1991) 3117.

- [3] M.A. Van Hove, R.J. Koestner, P.C. Stair, J.P. Bibérian, L.L. Kesmodel, I. Bartoš and G.A. Somorjai, *Surf. Sci.* 103 (1981) 189; 218.
- [4] E. Lang, K. Müller, K. Heinz, M.A. Van Hove, R.J. Koestner and G.A. Somorjai, *Surf. Sci.* 127 (1983) 347.
- [5] N. Bickel and K. Heinz, *Surf. Sci.* 163 (1985) 435.
- [6] Q.J. Gao and T.T. Tsong, *J. Vac. Sci. Technol. A* 5 (1987) 761.
- [7] K. Müller, J. Witt and O. Schültz, *J. Vac. Sci. Technol. A* 5 (1987) 757.
- [8] P.R. Norton, J.A. Davies, D.K. Creber, C.W. Sitter and T.E. Jackman, *Surf. Sci.* 108 (1981) 205.
- [9] M.A. Van Hove, W.H. Weinberg and C.-M. Chan, *Low-Energy Electron Diffraction: Experiment, Theory and Surface Structure Determination* (Springer, Berlin, 1986) p. 260.
- [10] D. Dunn, P. Xu and L.D. Marks, *Surf. Sci.* 294 (1993) 308.
- [11] P. Xu and L.D. Marks, *Ultramicroscopy* 45 (1992) 155.
- [12] L.D. Marks, *Ultramicroscopy* 38 (1991) 325.
- [13] K. Takayanagi, Y. Tanishiro, S. Takahashi and M. Takahashi, *Surf. Sci.* 164 (1985) 367.
- [14] J.M. Gibson, *Surf. Sci. Lett.* 239 (1990) L531.
- [15] L.D. Marks, *Ultramicroscopy* 45 (1992) 145.
- [16] J.M. Cowley and A.F. Moodie, *Acta Crystallogr.* 10 (1957) 609.
- [17] J.M. Cowley and A.F. Moodie, *Acta Crystallogr.* 12 (1959) 353.
- [18] J.M. Cowley and A.F. Moodie, *Acta Crystallogr.* 12 (1959) 360.
- [19] B.S. Garbow, K.E. Hillstrom, J.J. More, Argonne National Laboratory, Minpack Project, March 1980.
- [20] J.E. Dennis, D.M. Gay and R.E. Welsch, *ACM Trans. Math. Software* 7 (1981) 348.
- [21] P.G. Self, M.A. O'Keefe, P.R. Busek and A.E.C. Spargo, *Ultramicroscopy* 11 (1983) 35.
- [22] Y. Ma and L.D. Marks, *Acta Crystallogr.* 46 (1990) 11.
- [23] M.A. Metherell, in: *Electron Microscopy in Materials Science*, Vol. 2, Eds. U. Valdre and E. Ruedl (NATO Publications, Luxembourg, 1967) p. 397.
- [24] P.B. Hirsch, A. Howie, R.B. Nicholson, D.W. Pashley and M.J. Whelan, *Electron Microscopy of Thin Crystals* (Krieger, New York, 1977).
- [25] *High Resolution Transmission Electron Microscopy and Associated Techniques*, Eds. P.R. Busek, J.M. Cowley and L. Eyring (Oxford University Press, New York, 1988).
- [26] D.M. Bird and Q.A. King, *Acta Crystallogr. A* 46 (1990) 202.
- [27] W.C. Hamilton, *Acta Crystallogr.* 18 (1965) 502.
- [28] J.H. van der Merwe, *J. Appl. Phys.* 34 (1963) 117.
- [29] This paper only considers the tensile wave, and the shear wave can be readily obtained using the same general approach.
- [30] L.D. Marks, in preparation.
- [31] W. Moritz, F. Müller, D. Wolf and H. Jagodzinski, in: *Proc. 9th Vacuum Congr. and 5th Int. Conf. on Solid Surfaces*, Madrid (1980) p. 70.
- [32] K. Heinz, *Prog. Surf. Sci.* 27 (1988) 239.